

Rubble persistence under ocean acidification threatened by accelerated bioerosion and lower-density coral skeletons

Alice E. Webb^{1,2,3}  | Ana M. Palacio-Castro^{2,3} | Kenzie Cooke^{2,3} |
 Katherine R. Eaton³  | Benjamin Chomitz^{2,3} | Nash Soderberg^{2,3}  |
 Morgan Chakraborty³ | Zachary Zagon^{2,3}  | Albert Boyd^{2,3} | Patrick M. Kiel^{2,3} |
 Allyson DeMerlis^{2,3} | Chris T. Perry¹  | Ian C. Enochs²

¹Geography, College of Life and Environmental Sciences, University of Exeter, Exeter, UK

²Atlantic Oceanographic and Meteorological Laboratory, Ocean Chemistry and Ecosystem Division, NOAA, Miami, Florida, USA

³Cooperative Institute for Marine and Atmospheric Studies, University of Miami, Miami, Florida, USA

Correspondence

Alice E. Webb, Atlantic Oceanographic and Meteorological Laboratory, Ocean Chemistry and Ecosystem Division, NOAA, Miami, FL, USA.
 Email: alice.webb@noaa.gov; a.e.webb@exeter.ac.uk

Funding information

NOAA's Coral Reef Conservation Program; NOAA's Ocean Acidification Program; NOAA Omics Initiative

Abstract

As the balance between erosional and constructive processes on coral reefs tilts in favor of framework loss under human-induced local and global change, many reef habitats worldwide degrade and flatten. The resultant generation of coral rubble and the beds they form can have lasting effects on reef communities and structural complexity, threatening the continuity of reef ecological functions and the services they provide. To comprehensively capture changing framework processes and predict their evolution in the context of climate change, heavily colonized rubble fragments were exposed to ocean acidification (OA) conditions for 55 days. Controlled diurnal pH oscillations were incorporated in the treatments to account for the known impact of diel carbonate chemistry fluctuations on calcification and dissolution response to OA. Scenarios included contemporary pH (8.05 ± 0.025 diel fluctuation), elevated OA (7.90 ± 0.025), and high OA (7.70 ± 0.025). We used a multifaceted approach, combining chemical flux analyses, mass alteration measurements, and computed tomography scanning images to measure total and chemical bioerosion, as well as chemically driven secondary calcification. Rates of net carbonate loss measured in the contemporary conditions ($1.36 \text{ kg m}^{-2} \text{ year}^{-1}$) were high compared to literature and increased in OA scenarios (elevated: $1.84 \text{ kg m}^{-2} \text{ year}^{-1}$ and high: $1.59 \text{ kg m}^{-2} \text{ year}^{-1}$). The acceleration of these rates was driven by enhanced chemical dissolution and reduced secondary calcification. Further analysis revealed that the extent of these changes was contingent on the density of the coral skeleton, in which the micro- and macroborer communities reside. Findings indicated that increased mechanical bioerosion rates occurred in rubble with lower skeletal density, which is of note considering that corals form lower-density skeletons under OA. These direct and indirect effects of OA on chemical and mechanical framework-altering processes will influence the permanence of this crucial habitat, carrying implications for biodiversity and reef ecosystem function.

This is an open access article under the terms of the [Creative Commons Attribution](#) License, which permits use, distribution and reproduction in any medium, provided the original work is properly cited.

© 2024 The Author(s). *Global Change Biology* published by John Wiley & Sons Ltd.

KEY WORDS

bioerosion, calcification, coral density, coral reef, ocean acidification, rubble

1 | INTRODUCTION

The persistence of coral reefs relies on their capacity to maintain complex three-dimensional framework structures and retain their vertical growth potential. These attributes are necessary for reefs to sustain the continuity of their ecological functions and the irreplaceable services they provide (Graham & Nash, 2013). Beyond supporting an incredibly rich diversity of organisms, the heterogeneous calcium carbonate (CaCO_3) architecture of reefs plays a central role in attenuating wave energy, offering protection against shoreline erosion and mitigating the risk of flooding (Ferrario et al., 2014; Perry et al., 2018). This structure arises from the long-term accumulation of carbonate, derived from the calcification of corals and other calcifying organisms, which on average outpace the effects of physical, chemical, and biological breakdown processes (Perry et al., 2008).

In the natural biogeological development of coral reefs, erosion and subsequent rubble and sand generation are inherent and important processes (Perry & Hepburn, 2008). However, intensifying degradation and loss of habitat due to combined anthropogenic stressors have exacerbated erosion, threatening the delicate balance between constructive and erosional forces on contemporary reefs (Molina-Hernández et al., 2020; Perry et al., 2013). Today, many reefs exhibit diminished growth potential following transitions in community compositions and, going forward, may not be able to keep pace with rising sea levels (Kuffner et al., 2019; Perry et al., 2018; Webb et al., 2023; Yates et al., 2017). Numerous factors contribute to this precarious situation, and they range in scale from acute local or regional stressors to chronic global issues (Wolff et al., 2018).

The factors that impede coral calcification often also accelerate erosion, causing the balance between these opposing processes to shift in favor of net framework loss (Perry et al., 2008). Thermal anomalies causing large-scale coral mortality, for instance, leave substrate free for rapid colonization by opportunistic bioeroding species such as endolithic sponges (Chaves-Fonnegra et al., 2018). Ocean acidification (OA) is recognized to further accelerate the rate at which bioeroders chemically dissolve reef substrates while simultaneously reducing the rate at which many coral species can precipitate CaCO_3 (Enochs et al., 2016; Silbiger & Donahue, 2015). Waters enriched in nutrients and organic matter can impede coral health and calcification while providing an energy source for the excavating activities of heterotrophic bioeroders (DeCarlo et al., 2015; Holmes, 2000; Webb et al., 2017). As rates of erosion have begun to exceed rates of calcification, increasingly more framework is being reduced to coral rubble (Alvarez-Filip et al., 2009; Morris et al., 2022).

Today, coral rubble and the extensive beds they form are a common sight on reef landscapes. While their generation can have

lasting effects on reef communities and structural complexity (Kenyon et al., 2023; Rogers et al., 2018; Wolfe et al., 2021), they also provide an emerging complex microhabitat that can support a high density and diversity of reef organisms with varying functional roles (Enochs & Manzello, 2012). Regardless of whether dead standing corals remain affixed to the reef framework or break apart and transition into rubble, they undergo a continuous post-mortem transformation driven by a succession of multiphytic colonizers (Kenyon et al., 2023; Rasser & Riegl, 2002; Scoffin, 1992). Initially, a microbial biofilm grows over the newly dead coral, followed by the rapid colonization of epilithic and endolithic microorganisms including cyanobacteria, algae, and fungi (Sanchez-Quinto & Falcon, 2021). These primary colonizers lay the foundation for more complex organisms to slowly move in. As time progresses, various encrusting and macroboring invertebrates, such as sponges, bryozoans, worms, bivalves, and small crustaceans, settle in and alter this newly available habitat (Wolfe et al., 2021). It typically takes years (>5) before a mature internal bioeroder community is established (Kiene & Hutchings, 1994). Micro- and macro-boring taxa chemically and physically erode rubble fragments, while secondary calcifiers (non-coral calcifying invertebrates and calcareous algae) modify and encrust their surfaces, cementing pieces of detached reef together through calcareous overgrowth and thereby contributing to framework stability (Davidson et al., 2018; Enoch et al., 2021; Silbiger & Donahue, 2015). The significance of these opposing processes and their contribution to carbonate persistence will change and evolve as coral cover decline generates newly available substrate for these framework altering groups (Glynn & Manzello, 2015; Hughes et al., 2018). Kline et al. (2019) suggested that the pH threshold at which reefs transition into net dissolution is dependent on the ratio of living to dead coral on the reef.

As coral reefs shift toward having a greater relative abundance of rubble, it is imperative to advance our understanding of the role colonized dead coral fragments will play in future reef carbonate budgets (Romanó de Orte et al., 2021). Research on rubble fragments or rubble beds in the context of OA is limited. For instance, three studies robustly capture the effect of OA on Hawaiian rubble (Silbiger & Donahue, 2015; Stubler & Peterson, 2016; Yates & Halley, 2006), but each solely addresses a single aspect of bioerosion rather than considering the distinct impacts on the chemical and total components. More studies have concentrated on quantifying bioerosion rates by monitoring unaltered CaCO_3 blocks deployed on the reef for an extended period (Dee et al., 2023; Enoch et al., 2021; Silbiger & Donahue, 2015; Tribollet & Golubic, 2005). However, despite thoroughly documenting the impacts of initial colonization, these studies do not capture the erosive potential of a mature endolithic community, likely resulting in an underestimation of the ecologically relevant effects of macrobioerosion.

Our approach here, is to conduct a comprehensive examination of bioerosion and calcification rates within a well-established natural rubble community of bioeroders and secondary calcifiers. To explore the impacts of changing ocean chemistry, rubble fragments were placed in a dynamic OA replication system simulating diurnal pH oscillations, which has been shown to modulate both dissolution and calcification responses to OA (Enochs et al., 2018; Morris et al., 2022). The three different scenarios included contemporary pH (8.05 ± 0.025 pH diel fluctuation), elevated OA (7.90 ± 0.025), and high OA (7.70 ± 0.025). The future levels are broadly consistent with projections by 2050 and 2100 under SSP5-8.5 (van Hoidonk et al., 2020), which represent a plausible emission pathway associated with the world's economy heavily reliant on fossil fuel development (Taking the Highway) (Riahi et al., 2017). Our multifaceted approach, integrating physical, chemical, and digital techniques, allowed us to establish a holistic understanding of the framework altering processes of these increasingly significant rubble communities.

2 | MATERIALS AND METHODS

2.1 | Sample collection

Dead coral fragments colonized by multi-phyletic assemblages were collected by SCUBA at two sites in the Upper Florida Keys: Cheeca Rocks and Little Conch (depth: 3–5 m) on October 27, 2022. Cheeca Rocks (24.8966 N, 80.6169 W) is a patch reef off Islamorada characterized by regionally high coral cover (~25%) (Webb et al., 2023). The rubble samples were collected from dense rubble beds composed of branching *Porites* spp. Little Conch (24.9476 N, 80.4445 W) is a relatively flat reef off Plantation Key and is characterized by high turf and rubble cover and low coral cover. The collected rubble fragments from this location were morphologically different from those collected at Cheeca Rocks, originating from massive *Orbicella* spp. Only pieces of rubble without any live coral were collected. Ninety rubble fragments were selected for the experiment (*Porites* spp.=45, *Orbicella* spp.=45). The community observed on collected rubble included encrusting sponges, secondary calcifiers including CCA (crustose coraline algae), *Peyssonnelia* and *Halimeda*, non-encrusting invertebrates such as bivalves and small crustaceans, filamentous, and turf algae. Internal bioeroders included boring bivalves, sipunculids, phoronids, sponges (encrusting and boring), and a diverse assemblage of polychaete worms.

2.2 | Experimental design

Rubble fragments were placed in seawater filled tubs and transported (2.5-h transit) to the University of Miami Cooperative Institute for Marine and Atmospheric Studies (CIMAS) and the NOAA Atlantic Oceanographic and Meteorological Laboratory

(AOML) Experimental Reef Lab (ERL) where they were distributed across nine independent aquarium systems. Each rubble fragment was cleared of motile fauna (if present) and placed on the lid of a pre-tagged petri dish to enable identification of each individual fragment. A detailed description of the ERL aquaria setup can be found in Enochs et al. (2018). Briefly, it included completely independent aquaria systems (75 L glass tanks, 58 cm W × 58 cm L × 27 cm H), each with high-resolution, real-time control of pH and temperature. Incoming seawater was pumped from Biscayne Bay, UV sterilized, passed through 1 μm filter, and flowed into each tank system at a rate of 250 mL min⁻¹. Two mass flow controllers per tank control the venturi injection of CO₂ gas and CO₂-free air, while aquarium pH is measured using a solid-state pH electrode (Durafet, Honeywell). Temperature is measured using a high-resolution resistive temperature detector (TTD25C, ProSense) and maintained at a constant level via a 400W submersible heater and a solenoid-operated titanium chiller coil in each aquarium system. Each tank contains a high-intensity LED light array (EcoTech Marine Radion XR30 G5 Pro) that mimics natural diel fluctuations (peak photosynthetically active radiation of 250 mmol m⁻² s⁻¹) and a flow pump to mimic wave energy. Each tank system is controlled via custom computer algorithms and a graphical user interface, facilitating dynamic (time-dependent) treatments, controlled treatment ramping, and natural diel oscillations.

The rubble fragments were acclimated to the indoor laboratory setting for 10 days using conditions similar to those at their collection sites (27.5°C and 8.05 ± 0.02 pH diel fluctuation). The rubble was then exposed to a gradual 1-week pH ramping period to target treatment conditions. Treatments consisted of one contemporary (8.05 ± 0.025) and two future OA mean pH conditions (elevated: 7.90 ± 0.025 ; and high: 7.70 ± 0.025) representing potential mid and end of century conditions (IPCC; Pörtner et al., 2019). Three replicate tanks were used per treatment, with each tank containing five rubble pieces from each coral species ($n=10$ per tank), distributed at random in the tank space and turf facing upward. All treatments followed 24 h sinusoidal pH oscillations that mimicked natural reef environments (Albright et al., 2013), with minimum pH occurring at 06:00 h and maximum pH at 18:00 h. Treatment conditions were maintained for a total of 55 days.

Temperature and pH were logged every 5 min. Durafet pH electrodes were calibrated weekly using water samples analyzed for pH (8454 UV-Vis Spectrophotometer, Agilent Cary). Additionally, seawater samples (500 mL) were collected weekly from each tank for analysis of spectrophotometric pH, total alkalinity (A_T; Apollo SciTech, AS-ALK2), and dissolved inorganic carbon (DIC; Apollo SciTech, AS-C3) as per the manufacturer's guideline (two seawater replicates; calibrated with certified reference materials (batch# 198), Scripps Institution of Oceanography) (Dickson et al., 2007). Parameters were used to calculate other carbonate system variables such as pCO_2 (μatm) and aragonite saturation state (Ω_{arag}) using the package seacarb (Gattuso et al., 2015) in the R software environment (v4.3.0; R Core Team 2023).

2.3 | Response measurements

Following the acclimation period, each rubble piece was incubated in both light and dark conditions, computed tomography (CT) scanned, and buoyant weighed. Measurements were used to assess pre-treatment dissolution and calcification rates, as well as net production/respiration and nutrient uptake/release rates. These analyses were repeated after 55 days to quantify rubble response under the effect of OA.

2.3.1 | Rubble morphology

The surface area and volume of each rubble fragment were determined by non-destructive CT using a Siemens SOMATOM Volume Zoom set to a 0.1 mm slice width and spiral scan. Rubble samples were maintained in seawater throughout the scanning process, both before and after the duration of the experiment. CT scans were reconstructed from image stacks using Amira (Thermo Fisher Scientific, Massachusetts, USA). Custom-made coral aragonite density reference materials were analyzed throughout the scanning process, using the same scan and reconstruction parameters. The skeletal density of rubble samples was inferred from grayscale values by linear regression of coral standards of known density (*Porites lobata*: 1.1285 g cm⁻³, *Pseudodiploria clivosa*: 1.568 g cm⁻³ and *Acropora palmata*: 2.0630 g cm⁻³) (Groves et al., 2018; Manzello et al., 2018, 2021). Surface areas and volumes of pre- and post-scans were measured by creating three-dimensional isosurfaces following the boundary between the water and each rubble piece using Amira. Orthogonal slice images were generated to confirm rubble coral species and to verify the presence of a well-established community of macro-bioeroders.

2.3.2 | Short-term incubations

Each rubble fragment was placed separately into custom-built, clear and dark acrylic incubation chambers (0.75 L) to represent the two light treatments (light and dark). The chambers were placed on submersible stirring units in the aquaria for temperature control. Each stirring unit contained a submersible motor that created continuous water movement in each chamber via magnetic stir bars. Every incubation spanned a duration of 2 h and water samples were collected prior to and after the incubation period to determine initial and final water conditions. Initial water conditions were sampled immediately before each round of incubations by collecting bulk tank treatment water including 40 mL for nutrients analysis, 250 mL for analysis of A_T, and 175 mL for the analysis of pH, density and DIC. After 2 h, chambers were opened, and subsamples were taken from each chamber to determine post-incubation water conditions. Samples for A_T, pH, and DIC were preserved in sealed borosilicate bottles with mercury chloride (6.5%) (150 and 100 µL HgCl₂ for 250 and 175 mL samples respectively). From the

250 mL sample for the determination of A_T, two replicate filtered water samples (each 50 g) were analyzed within 36 h of collection using a potentiometric titrator (Metrohm 855 Robotic Titrosampler equipped with 800 Dosino pump and Tiamo software). If A_T values for replicates were more than 4 µmol apart, a third replicate (from the same sample origin) was analyzed. Analytic precision, determined from absolute differences in measurements between replicates, was ~1.4 ± 0.9 µmol (mean ± SD). The mean of replicates was used for further calculations. The 40 mL samples for determination of all nutrients (including nitrate, nitrite, phosphate and ammonium) were filtered through 0.45 µm Acrodisc filters during collection and stored frozen until analysis was carried out on a SEAL AutoAnalyzer 3. Oxygen measurements were performed with the Witrox 4 O₂ meter (Loligo Systems) in bulk tank seawater before incubations and after 2 h in each incubation chamber. Control incubations, containing seawater but no rubble samples, were performed in replicate for each treatment and light level ($n=4$ pre-treatment and $n=12$ post-treatment) to correct calcification/dissolution signals from rubble incubations. Defaunated clean rubble fragments were not used as controls as they quickly become colonized by microorganisms and any chemical signal recorded from these incubations would not accurately represent processes from the community that was being evaluated.

2.3.3 | Long-term mass change

Each rubble fragment was weighed pre, mid and post-experiment using the buoyant weight technique (Dodge et al., 1984; Spencer Davies, 1989) within a temperature-controlled seawater tank. Samples were suspended on a stainless-steel platform attached to the analytical balance with hydrophobic tungsten wire (0.05 mm). Mass was measured using a calibrated analytical balance (0.0001 g precision, Ohaus). Prior to each measurement, temperature and salinity were recorded by a high-accuracy temperature probe (model, Digi-Sense).

2.4 | Rates

2.4.1 | Short-term incubation processes

Net chemical dissolution/calcification

Rates of dissolution and calcification were determined using the alkalinity anomaly technique (Chisholm & Gattuso, 1991; Smith & Key, 1975) involving measured changes in A_T associated with dissolution or precipitation in seawater during 2 h incubation. Concurrent measured changes in nutrient concentration were used to correct A_T change (Jacques & Pilson, 1980; Wissak et al., 2013) as ammonium, nitrate and phosphate are naturally modified by the rubble inhabitants and affect A_T. The mass of altered calcium carbonate (ΔM_{CaCO_3} , in µg) was calculated using the equation below (Zundelovich et al., 2007):



$$\Delta M_{\text{CaCO}_3} = 0.5 \times [\Delta A_T + \text{PO}_4 - \text{NH}_4 + (\text{NO}_3 + \text{NO}_2)] \times V_{\text{SW}} \\ \times \rho_{\text{SW}} \times 100,$$

where ΔA_T is the change in A_T over the incubation period associated with dissolution/precipitation, V_{SW} is the volume (L) of seawater in the incubation chamber (minus rubble volume) and ρ_{SW} is seawater density ($\sim 1022 \text{ kg m}^{-3}$). The multiplication factor "100" represents the molecular mass of CaCO_3 . Rates are commonly expressed as mass of removed/gained substrate per unit surface area of the removing organism per unit of time. However, due to the internal nature of bioerosion and since the rubble from each location had similar average surface areas but varying volumes, we standardized the rates to rubble volume instead ($\text{mg cm}^{-3} \text{ h}^{-1}$). For ease of comparison with existing literature in the discussion, we still standardized rates to surface area while noting that due to the varying surface-to-volume ratios among rubble fragments, this resulted in a pronounced difference in results between the two rubble coral species and likely led to an underestimation of rates. Net calcification over 24 h was calculated as the sum of 12 dark h and 12 light h.

Net production, respiration, and nutrient cycling

As outlined above, measurements of A_T were corrected for the effect of nutrient release by respiration. The contribution of DIC to respiration can be quantified because respiration derived DIC does not impact ΔA_T and calcification/dissolution modifies the A_T :DIC at a 2:1 ratio. The contribution of respiration to the observed DIC concentrations was calculated as follows:

$$\begin{aligned} \Delta A_T^{\text{diss}} &= \Delta A_T^{\text{obsNC}} && \text{change in } A_T \text{ due to dissolution with } ^{\text{obsNC}} \\ &&& \text{adjusted for nutrients,} \\ \Delta A_T^{\text{resp}} &= 0 && \text{change in } A_T \text{ due to respiration,} \\ \Delta \text{DIC}^{\text{diss}} &= \Delta A_T^{\text{obsNC}} / 2 && \text{change in DIC due to dissolution,} \\ \Delta \text{DIC}^{\text{resp}} &= \Delta \text{DIC}^{\text{obs}} - \Delta \text{DIC}^{\text{diss}} && \text{change in DIC due to respiration,} \end{aligned}$$

where $\Delta \text{DIC}^{\text{resp}}$, ΔO_2 , and Δ nutrients rates (in $\mu\text{mol kg}^{-1} \text{ h}^{-1}$) were converted to fluxes ($\mu\text{mol cm}^{-2} \text{ h}^{-1}$), with an enclosed water volume of $\sim 0.75 \text{ L}$ (minus rubble volume) (seawater density $\sim 1022 \text{ kg m}^{-3}$) and each respective rubble volume.

2.4.2 | Long-term bioerosion

Total bioerosion

Total bioerosion rates were determined using the buoyant weight technique (Dodge et al., 1984). Temperature and salinity were used to calculate seawater density and convert buoyant weight to total skeletal mass. As with the incubations, changes in mass were standardized to rubble volume, obtained from CT scans. This method usually assumes organic components of the coral skeleton to have a density equal to

that of the ambient seawater (i.e., growth of sponge or algal tissue would not change the buoyant weight) (Dodge et al., 1984). Here, rubble pieces may have been colonized by calcareous organisms that produce more additional surficial carbonates. As such, our measurements of rubble erosion are potentially conservative underestimates.

Mechanical bioerosion

Mechanical bioerosion by macroborers was calculated by subtracting chemical bioerosion from total bioerosion (Schönberg et al., 2017).

2.5 | Statistical analysis

2.5.1 | Rubble coral species morphology

Statistical analyses were performed using the R software (R Core Team, 2020). Variations in morphological attributes (densities, volumes, and surface area) between the two rubble coral species and scenarios were assessed using generalized linear models (GLMs). GLMs with Gaussian distribution were run using the package 'glm-mTMB' (Brooks et al., 2017). For post-treatment density, a generalized linear mixed model (GLMMs) was run with tank as a random effect. All model residuals were diagnosed using the package "DHARMa" (Hartig, 2020). Final models were then checked for overdispersion and zero-inflation; none of the final models required correction.

2.5.2 | Short-term incubation processes

GLMMs were run to examine the effects of pH, light, rubble coral species on post-treatment chemically quantified incubation response metrics (calcification/dissolution rates, photosynthesis, respiration, nutrient fluxes). Tank was treated as a fixed random effect. Two types of GLMMs were employed based on the distribution of the data examined, either Gaussian (identity link function) or Gamma (log link function). Response variables analyzed with Gamma GLMMs which contained negative values were shifted before analysis and then transformed back to original before graphing.

GLMMs with Gaussian distribution were also run to examine pre-treatment hourly and 24 h calcification/dissolution rates and compare them to contemporary post-treatment rates. Light and rubble coral species were set as fixed effects and tank and rubble ID as fixed random effect.

Three GLMMs with Gaussian distribution were conducted to look at the effect of rubble density on 24 h chemical calcification and dissolution rates. The first model incorporated rates from all pH scenarios, rubble coral species, and density as fixed effects. Subsequently, two additional GLMMs were performed, separating data from contemporary and OA scenarios. In all three models, the factor 'tank' was included as a random effect

For all GLMMs, residuals were diagnosed using the package "DHARMa" and final models were checked for overdispersion and zero-inflation.

2.5.3 | Long-term bioerosion

Additional GLMMs were run to examine the effect of OA treatment, rubble coral species and density on 24h mechanical and total bioerosion rates. Tank was again treated as a fixed random effect. Both mechanical and total bioerosion rates were analyzed using Gamma distribution after all rates were shifted to positive. Residuals were also diagnosed using the package "DHARMA". Final models were then checked for overdispersion and zero-inflation; none of the final models required correction.

3 | RESULTS

3.1 | Carbonate chemistry across treatment

Target pH values for the three treatments were reached after 1 week ramping and were maintained throughout the experiment (Table 1; Figure 1). Durafet probe error, calculated as the difference between measured pH (Durafet) and spectrophotometric pH determined from water samples revealed that the probes were stable and accurate throughout the experiment (standard deviation contemporary=0.059; elevated=0.047; high=0.027). Variability in measured and calculated carbonate chemistry parameters were as expected, and nutrient concentration across treatments were comparable (Table 1).

3.2 | Rubble morphology

Orthogonal slice images of each rubble piece revealed high levels of bioerosion in every fragment (Figure S1). Worm scars and bivalves were the predominant traces in the scans (Figure 2c,d,e,f), as well as sponge bioerosion pits (Figure 2e, bioerosion pattern at the surface of the coral skeleton). The orthogonal slice images from

Little Conch rubble revealed that three fragments (two from the high treatment and 1 from the elevated one) originated from brain corals, rather than *Orbicella* spp. These fragments had lower densities and were removed from further analysis. The average pre- and post-experiment density of the *Porites* rubble (Cheeca Rocks) fragments were 1.62 ± 0.10 and $1.54 \pm 0.10 \text{ g cm}^{-3}$ and was comparable to the *Orbicella* rubble (Little Conch), which was 1.67 ± 0.14 and $1.59 \pm 0.15 \text{ g cm}^{-3}$. Pre- and post- densities of rubble in the elevated scenario were found to be on average lower (*Porites*: 1.58 ± 0.08 to $1.52 \pm 0.10 \text{ g cm}^{-3}$; *Orbicella*: 1.60 ± 0.12 to $1.52 \pm 0.12 \text{ g cm}^{-3}$, see Figures S2 and S3) than other rubble pieces despite random assignment of each rubble fragment to each treatment but this was not found to be significant (Table S2). Average surface area between coral types or treatments was not significantly different between *Porites* rubble ($98.2 \pm 17.5 \text{ cm}^2$) and *Orbicella* fragments ($95.0 \pm 12.1 \text{ cm}^2$). Volume was significantly different between coral types (GLM, $z=6.185$, $p<.001$) with an average volume of $40.2 \pm 10.7 \text{ cm}^3$ for *Porites* rubble and $54.9 \pm 10.8 \text{ cm}^3$ for *Orbicella* rubble (Figure S2; Table S2). This difference was not significant between treatments.

3.3 | Short-term incubation processes

3.3.1 | Calcification and dissolution rates

Daily and hourly rates of net calcification/dissolution in the pre-treatment incubations did not differ significantly from the rates in the contemporary post-treatment (Table S3). Post-treatment rates differed significantly from pre-treatment rates (GLMM, $z=10.319$, $p<.001$), between OA treatments (GLMM, $p<.001$), but not between rubble species. Light and dark hourly carbonate alteration differed from each other in both pre-treatment and post-treatment phases (GLMM, pre: $z=14.389$, $p<.001$; post:

Aquaria	Contemporary	Elevated	High
Temp (°C)	27.5 ± 0.02	27.5 ± 0.07	27.5 ± 0.05
Salinity	34.82 ± 0.65	34.78 ± 0.64	34.74 ± 0.64
A_T ($\mu\text{mol kg}^{-1}$)	2425 ± 25	2424 ± 24	2425 ± 21
pH _t	8.06 ± 0.07	7.90 ± 0.04	7.70 ± 0.08
pCO ₂ (μatm)	414 ± 79	640 ± 72	1094 ± 170
CO ₃ ²⁻ ($\mu\text{mol kg}^{-1}$)	252.4 ± 36.3	189.4 ± 19.4	129.7 ± 25.7
HCO ₃ ⁻ ($\mu\text{mol kg}^{-1}$)	1849 ± 68.5	2007 ± 46.0	2152 ± 71.3
DIC ($\mu\text{mol kg}^{-1}$)	2112 ± 487.7	2214 ± 40.9	2311 ± 54.8
Ω_{arag}	4.06 ± 0.59	3.05 ± 0.31	2.09 ± 0.42
NO ₂ ⁻ ($\mu\text{mol L}^{-1}$)	0.11 ± 0.19	0.11 ± 0.08	0.10 ± 0.03
PO ₄ ³⁻ ($\mu\text{mol L}^{-1}$)	0.049 ± 0.037	0.060 ± 0.030	0.042 ± 0.015
Si(OH) ₄ ($\mu\text{mol L}^{-1}$)	3.74 ± 2.19	4.38 ± 1.50	3.84 ± 1.27
NH ₄ ⁺ ($\mu\text{mol L}^{-1}$)	0.37 ± 0.36	0.46 ± 0.40	0.34 ± 0.20
NO ₃ ⁻ ($\mu\text{mol L}^{-1}$)	0.34 ± 0.30	0.57 ± 0.36	0.42 ± 0.62

TABLE 1 Mean and standard deviation of all weekly measured parameters throughout the experiment (55 days). $p\text{CO}_2$, HCO_3^- , CO_3^{2-} , and Ω_{arag} were calculated from the measured total alkalinity (A_T) and dissolved inorganic carbon (DIC) samples using Seacarb.

FIGURE 1 pH (total scale) measured in each tank for each hour within the diurnal cycle averaged across the 55 days of treatment conditions. The three treatment groups include mean $\text{pH} \pm \text{amplitude}$ of diel pH oscillations: 8.05 ± 0.025 , 7.90 ± 0.025 , 7.70 ± 0.025 . For each treatment, data from each replicate tank were pooled together and used to calculate the mean pH for each hour point. Error bars around each point depict standard deviation. Each shape represents one of the tank replicates in each pH treatment ($n=55$).

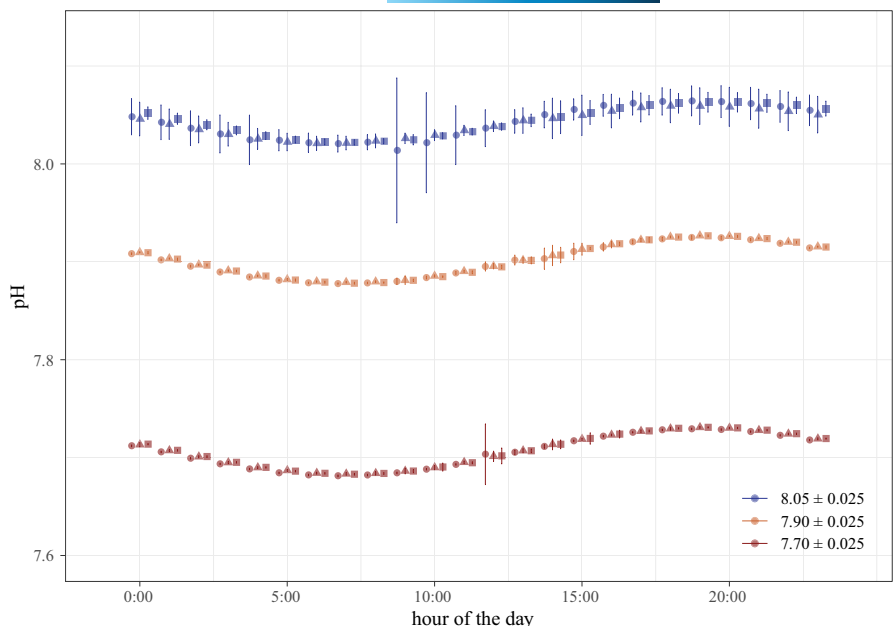
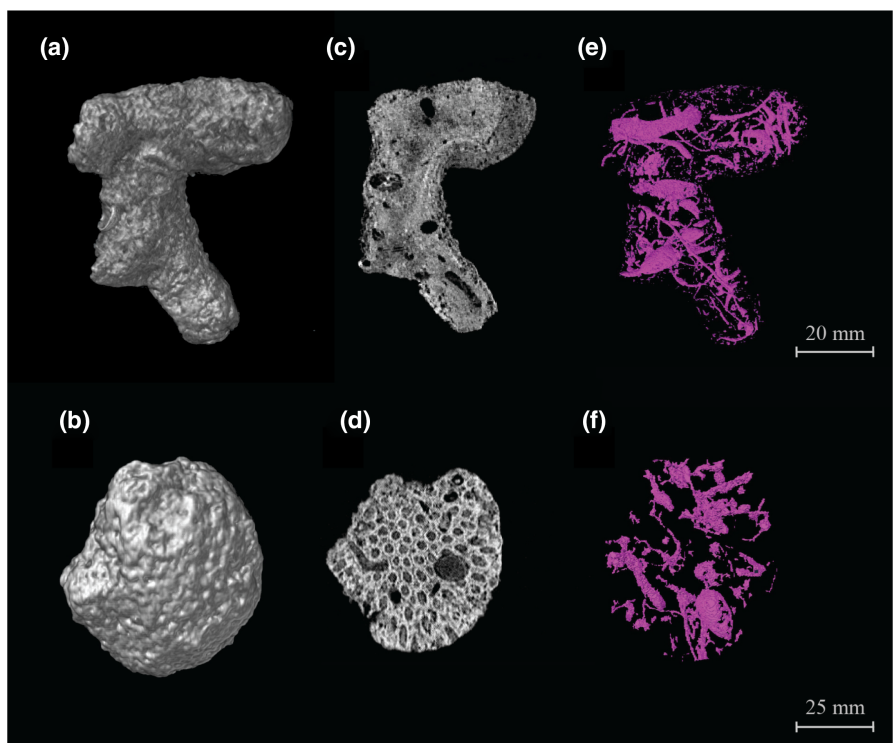


FIGURE 2 CT scans of coral rubble showing 3D reconstructions (a, b), orthogonal slices (c, d), and bioerosion traces (e, f) from two example rubble samples; a *Porites* spp. (top) and an *Orbicella* spp. (bottom) fragment collected at Cheeca Rocks and Little Conch reefs, respectively.



$z=19.766$, $p < .001$). Net calcification rates decreased in light incubations with decreasing pH, while net dissolution increased in dark ones. This led to a shift from net daily calcification (standardized across 24 h) in the contemporary treatment to net dissolution past a pH of 7.96 for *Porites* rubble and 7.98 for *Orbicella* rubble (Figure 3). An interaction between light regime and rubble coral species was found indicating that light affected rates from the two rubble species differently (GLMM, Light \times coral species: $z=-3.49$, $p = <.001$).

Net daily calcification in the pre-treatment phase was not significantly different between rubble coral species (or locations)

but was higher on average in *Porites* spp. ($0.070 \pm 0.127 \text{ mg cm}^{-3} 24 \text{ h}^{-1}$) versus *Orbicella* spp. ($0.027 \pm 0.127 \text{ mg cm}^{-3} 24 \text{ h}^{-1}$). Rates of net calcification decreased under the OA scenarios (pre- vs. elevated post-experiment; *Porites* spp.: 0.12 ± 0.15 to -0.07 ± 0.08 and *Orbicella* spp.: 0.02 ± 0.05 to $-0.07 \pm 0.06 \text{ mg cm}^{-3} 24 \text{ h}^{-1}$). Rates decreased even further in the high OA treatment (pre- vs. high post-experiment; *Porites* spp.: 0.05 ± 0.11 to -0.09 ± 0.08 and *Orbicella* spp.: 0.04 ± 0.06 to $-0.13 \pm 0.07 \text{ mg cm}^{-3} 24 \text{ h}^{-1}$). Net dissolution rates increased in higher density rubble ($z = -2.339$, $p = .019$) but only in the contemporary scenario (see section 3.4).

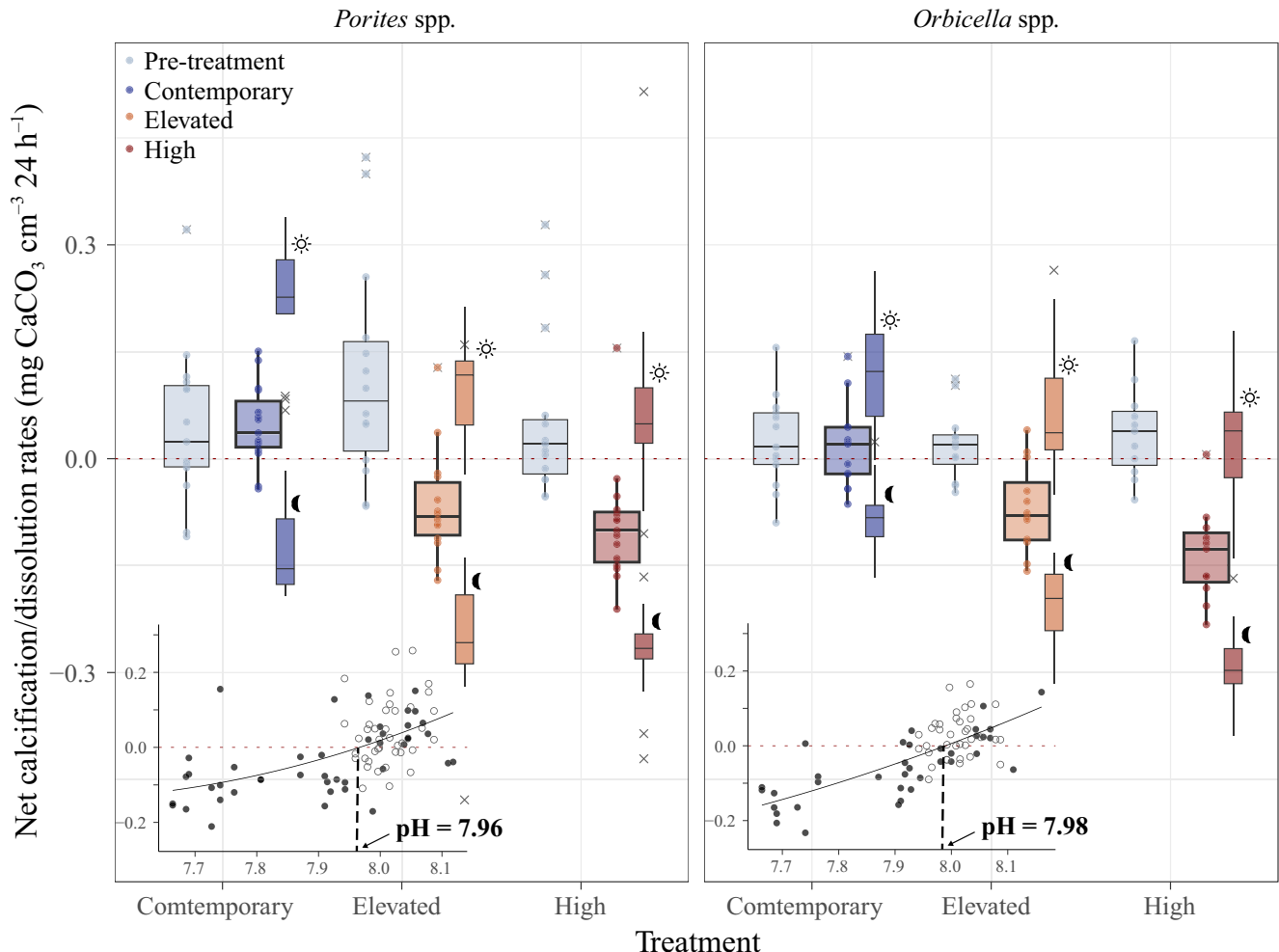


FIGURE 3 Chemical accretion and dissolution rates ($\text{mg CaCO}_3 \text{ cm}^{-3} 24 \text{ h}^{-1}$) of *Orbicella* spp. (Little Conch) and *Porites* spp. (Cheeca Rocks) rubble pieces before treatment (pale blue boxplots) and post treatment (contemporary in blue, elevated in orange and high in red). Net chemical rates over 24 h represent the sum of dark and light rates over 12 h (photoperiod = 12:12) (wider boxplots). The post-treatment net 24 h-standardized chemical rates are represented in bold. Net dark (moon) and light (sun) rates are represented by the thinner boxplot and were calculated by multiplying the hourly rate by 24. The two regression lines at the bottom represent net 24 h-standardized chemical rates (in $\text{mg CaCO}_3 \text{ cm}^{-3} 24 \text{ h}^{-1}$) versus pH measured in the incubation chambers. They indicated the threshold pH at which rubble fragments shift from net calcification to net dissolution. Circles depict pre-treatment data and black points show post-treatment data.

3.3.2 | Net production, respiration, and nutrient cycling

Net community calcification (NCC) increased with net community production (NCP). In general, rubble communities were net photosynthesizing and net calcifying during the day (Figure 4: circle in the upper right quadrants) and were net respiring and net dissolving at night (Figure 4 triangles in the lower left quadrants). Some exceptions were communities in the OA treatments: photosynthesizing and dissolving during the day (lower right quadrants). A few communities residing in the *Porites* rubble calcified at night while net respiring (upper left quadrant). Overall, NCP and NCC processes occur over a broader range in *Porites* rubble compared to the communities inhabiting *Orbicella* rubble.

OA treatments did not have a significant impact on net community respiration (NCR) and NCP rates (Table S3). NCP differed significantly between rubble species (GLMM, $z=4.93$, $p<.001$)

with *Orbicella* spp. having lower O₂ production rates during light incubations (GLMM, Light \times *Orbicella* spp., $z=-6$, $p<.001$). NCR did not differ significantly between species, but the factor light was also found to impact species differently with higher NCR measured in *Orbicella* spp. light incubations (i.e., less uptake of DIC occurred).

NO₂ and NO₃ fluxes were significantly different between dark and light incubations (Figure 5). Both *Porites* and *Orbicella* rubble took up less NO₂ during dark incubations (GLMM, $z=-4.483$, $p<.001$) and switched from being a source of NO₃ in dark incubations overall to being a sink in light ones (GLMM, $z=-2.647$, $p<.008$). Uptake of NO₂ was lower for *Orbicella* rubble during light incubations (Light \times *Orbicella* spp., $z=2.628$, $p<.009$). Significant reduced production and increased uptake of NO₃ occurred in the high OA scenario for both rubble coral species (GLMM, High: $z=-3.044$, $p=.002$). NH₄ fluxes increased on average in OA treatments, especially in *Orbicella* rubble, but this was not significant (Figure 5).

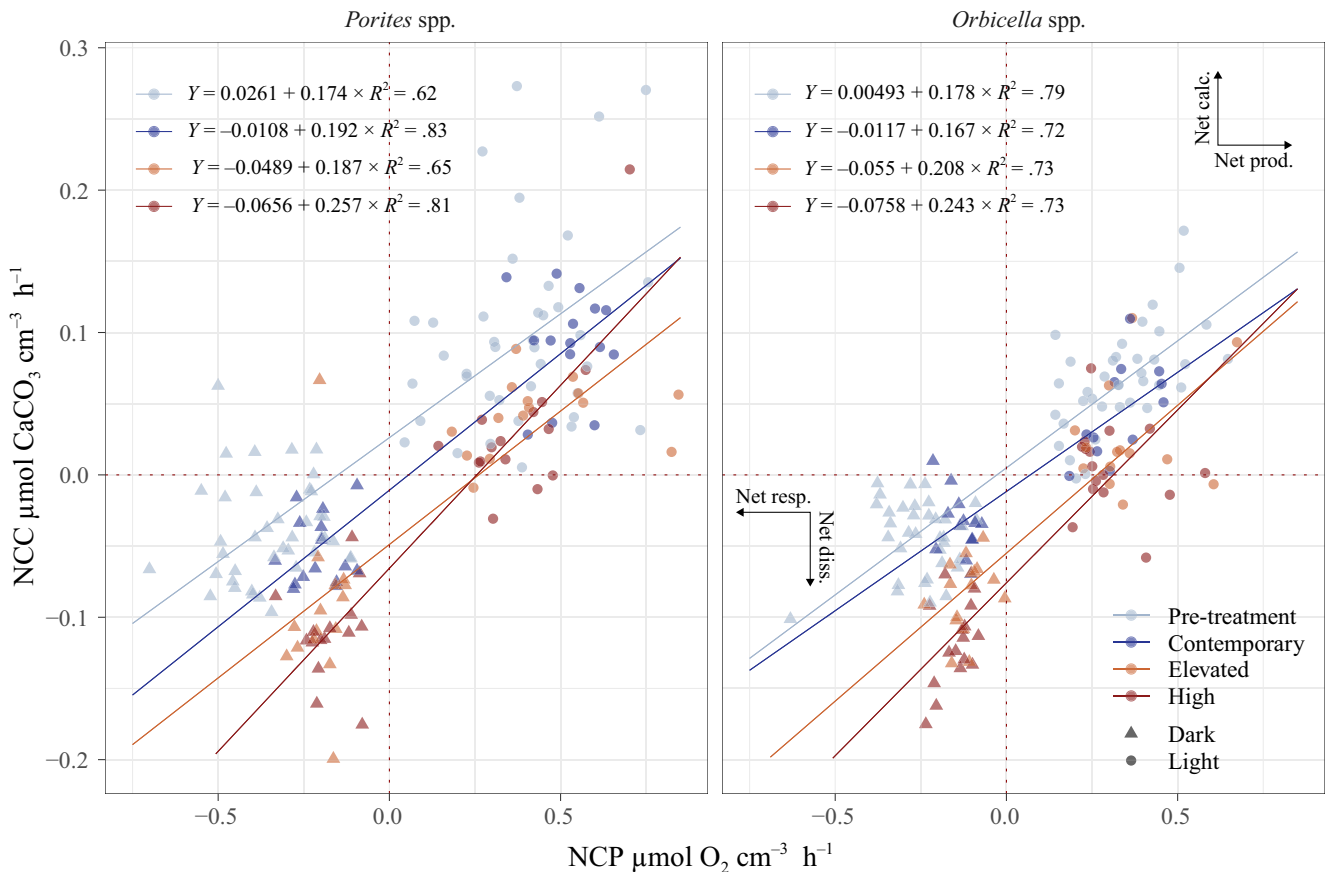


FIGURE 4 Net community calcification (NCC) and net community respiration measured from the difference in A_T and DIC respectively. Circles and triangles represent day and night rates respectively. Pale blue color represents data collected before the rubble was put in treatment (pre-treatment) and blue, orange and red colors depict rates measured after 55 days in treatment (post-treatment). Negative and positive y values show net dissolution and net calcification, respectively. Negative and positive x-axis values are net respiration and net photosynthesis. A_T , total alkalinity; DIC, dissolved inorganic carbon; NCP, net community production.

3.4 | Long-term bioerosion rates

Total bioerosion rates differed between coral types (GLMM, $z=3.923$, $p=.036$) and pH treatments (GLMM, elevated: $z=2.22$, $p=.0264$; high: $z=2.007$, $p=.0447$) (Table S4). They increased under the two OA scenarios (Figure 6) with the highest values recorded in the elevated scenario (-0.86 ± 0.56 and $-1.18 \pm 0.35 \text{ mg cm}^{-3} 24 \text{ h}^{-1}$ for *Porites* and *Orbicella* rubble respectively). Total bioerosion and its mechanical component (calculated by subtracting chemical rates from total rates) increased in lower density rubble (GLMM, total: $z=-6.1171$, $p<.001$; mechanical: $z=7.202$, $p<.001$) but mechanical bioerosion rates did not differ significantly between pH treatments and rubble coral species (Figure 7).

4 | DISCUSSION

In all scenarios, rubble fragments underwent net CaCO_3 loss during the experiment due to bio-erosional processes outpacing calcification. Our findings indicate that contemporary internal bioerosion in heavily colonized coral rubble was high compared to previous reports (Davies

& Hutchings, 1983; Osorno et al., 2005; Yeung et al., 2021) and will increase in a higher CO_2 world with severe implications for net reef framework persistence. Contemporary net total bioerosion averaged at 0.83 and $1.88 \text{ kg m}^{-2} \text{ year}^{-1}$ for *Porites* and *Orbicella* fragments, respectively, which suggest they contributes significantly to carbonate budgets, especially on degraded reefs. These high rates of bioerosion hold particular significance in regions like Florida, where most reefs are either experiencing net erosion or are in a state of stasis (Morris et al., 2022).

4.1 | OA enhanced bioerosion rates

Net bioerosion rates increased under OA conditions compared to the contemporary scenario. This acceleration was chemically driven with enhanced dissolution and reduced secondary calcification.

4.1.1 | Chemical dissolution and calcification rates

Results from rubble incubations in different pH treatments indicated that the ongoing increase in pCO_2 increase in the earth's

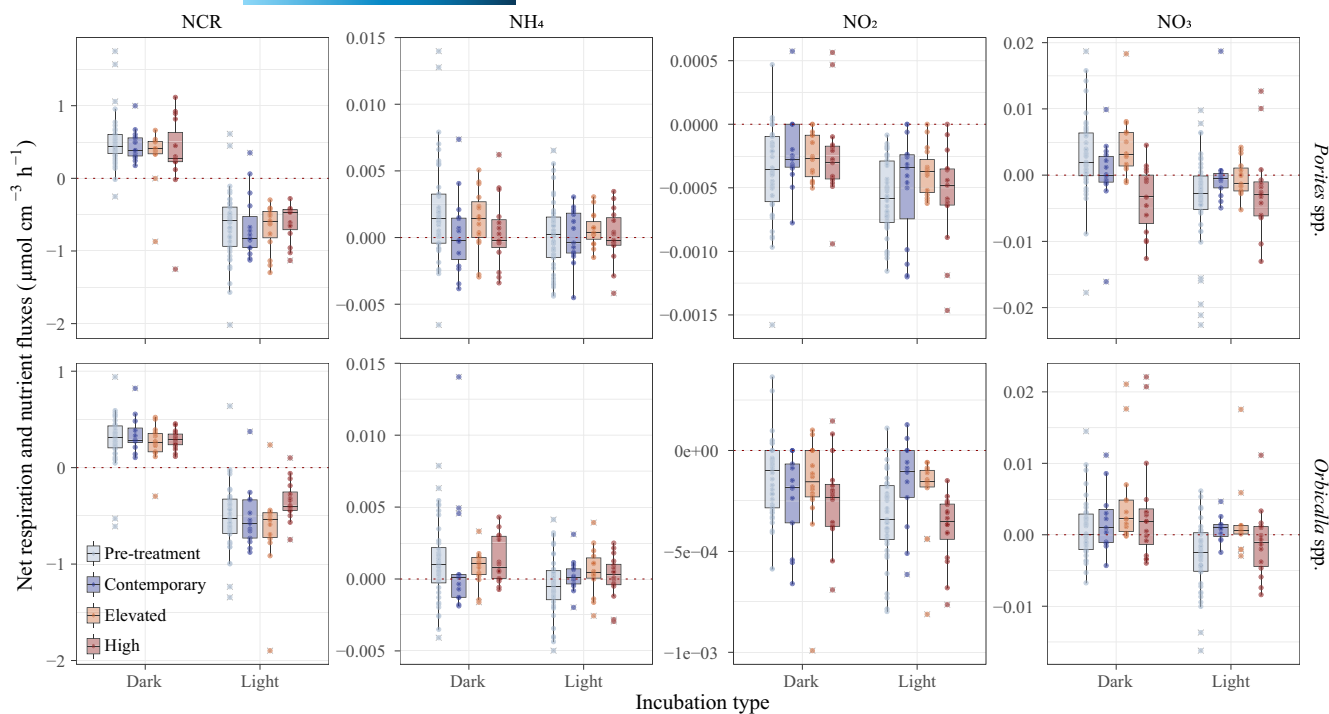


FIGURE 5 Boxplots depicting net community respiration (NCR) and net nutrient fluxes (in $\mu\text{mol cm}^{-3} \text{h}^{-1}$) recorded during light and dark incubations. The pre-treatment rates are depicted in the light blue boxplots and the rates measured post-treatment; after rubble were placed either in the contemporary, elevated, or high scenarios, are depicted by blue, orange, and red boxplots.

atmosphere will cause epi- and endolithically colonized coral rubble to shift from net calcification to net dissolution. The tipping point in this study, where rubble fragments, on average, transitioned into net dissolution, was met at pH = 7.96–7.98. These levels are predicted to be reached in the early 2040s under SSP5-8.5 (van Hoiddonk et al., 2020). Here, rates ranged from 0.001 to 0.004 $\text{mg cm}^{-3} \text{h}^{-1}$ during light incubations and -0.002 to 0.008 $\text{mg cm}^{-3} \text{h}^{-1}$ during dark incubations (light: 1.05 to 8.85 $\text{mmol CaCO}_3 \text{ m}^{-2} 24 \text{ h}^{-1}$; dark: -5.15 to -15.9 $\text{mmol CaCO}_3 \text{ m}^{-2} 24 \text{ h}^{-1}$), which was comparable with previous alkalinity anomaly studies on rubble from both experimental settings (Silbiger & Donahue, 2015) and in situ studies (Yates & Halley, 2006). It is of note however, that rates from the current study were normalized to the surface area of each rubble, while Silbiger and Donahue (2015) normalized rates to the surface area of an assemblage of rubble, and Yates and Halley (2006) normalized their rates to planar surface area.

Net calcification rates recorded on/in rubble were negatively correlated with OA. Previous studies investigating the response of polychaetes, molluscs, and CCA to acidification have found that they respond negatively to decreases in pH (Diaz-Pulido et al., 2012; Kuffner et al., 2008) due to chemical conditions not being conducive to CaCO_3 precipitation. Net dissolution rates, on the other hand, increased as pH lowered. Rates of chemical dissolution have been shown to increase with OA for bioeroders whose boring activity include a chemical component. Excavating sponges for instance, dissolve coral skeleton around a fragment of CaCO_3 , termed a chip, and then remove it mechanically (Webb et al., 2019). Enochs et al. (2016) found a positive relationship between the

boring activity of annelids and OA. While the mechanisms of carbonate dissolution are not well known for all annelid taxa, similar to boring bivalves, they are likely to involve both chemical dissolution and mechanical abrasion (Davies & Hutchings, 1983; Schönberg et al., 2017). Reduced pH would be conducive to easier dissolution by both mechanisms.

4.1.2 | Total and mechanical bioerosion

Incubation based rates represent the chemical component of all processes altering the rubble framework (only 7%–14% in *Porites* rubble and 4%–17% in *Orbicella* rubble of total mass change was due to dissolution) and they are not inclusive of the dominant influence of mechanical erosion resulting from macroboring taxa. Net total erosion of rubble (chemical+mechanical) already occurred in contemporary pH. This points to the importance of the contribution of macroborers that utilize non-chemical dissolution techniques to enter the substrate. Worm and bivalve mechanical bioerosion, as well as the mechanical chip production component of sponge bioerosion surpassed net calcification even in the contemporary treatment, where net total bioerosion rates reached an average of 0.2 and 0.3 $\text{g cm}^{-3} \text{year}^{-1}$ for *Porites* and *Orbicella* fragments respectively. Mechanical bioerosion was not significantly impacted by pH but increased significantly as density decreased. This resulted in highest bioerosion being recorded under the elevated scenario. Total bioerosion was therefore affected both by pH from its chemical component and density from its mechanical component.

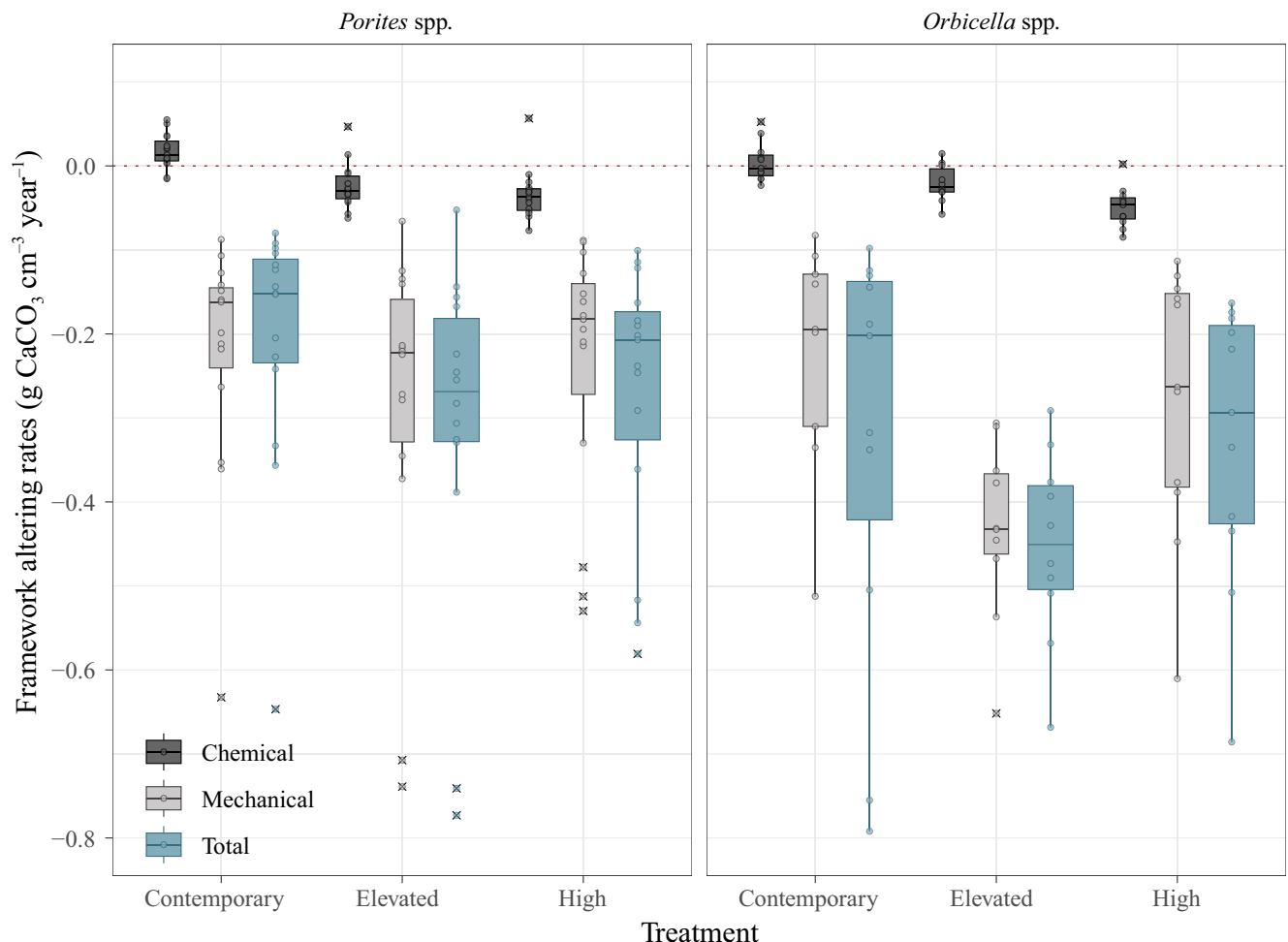


FIGURE 6 Boxplot depicting chemical (post-treatment), mechanical, and total framework altering rates in $\text{g CaCO}_3 \text{cm}^{-3} \text{year}^{-1}$ in the 3 pH scenarios. Chemical rates are converted from hourly to yearly for the purposes of comparison, and values should be treated with caution given the disparity in temporal resolution.

4.2 | Impact of density on bioerosion rates

The effect of density on bioerosion has been discussed in previous studies with mixed results. This is mostly due to different micro- and macro-eroding taxa having different bioerosion techniques resulting in varying responses to the density of the skeleton they inhabit. While some studies have found no significant correlation between micro- or macrobioerosion rates and coral skeletal densities (DeCarlo et al., 2015; Tribollet et al., 2002; Tribollet & Golubic, 2005), others focusing only on excavating sponges consistently found a positive correlation (Hernández-Ballesteros et al., 2013; Highsmith et al., 1983). At similar sponge tissue growth rates, denser materials would require the removal of a greater mass of material compared to more porous substrates. Molina-Hernández et al. (2022) investigated the impact of external bioerosion on recently deceased coral heads and found greater loss of substrate height on corals with lower density; the loss being attributed mostly to grazing by parrotfish. Conversely, some studies focusing on internal macroboring as a whole (e.g., by bivalves, worms, sponges) suggested that bioerosional damage to reef

corals was positively correlated with skeletal density (Cosain-Díaz et al., 2021; Hernández-Ballesteros et al., 2013; Highsmith, 1981; Highsmith et al., 1983; Hutchings, 1986). This relationship was explained by bioeroders preferring to settle on and penetrate denser corals for protection. It is important to highlight that in most of these studies, boring sponges accounted for more than 70% of the skeletal excavation. Additionally, some of these studies quantified bioerosion in live corals which would impact colonizing capacity by micro and macroborers (Holmes, 2000). Moreover, the aforementioned studies used bioerosional damage to quantify the volume and percentage of CaCO_3 removed through bioerosion, whereas in this study we quantify the real-time rate at which bioeroding communities remove coral skeleton mass. This likely explains the different findings; it is possible that worms and bivalves prefer settling on denser coral skeletons for protection, but that their mechanical boring activity is facilitated in less dense material.

The chemical component of the overall bioerosion by macroborers represents a relatively small percentage (4%–17% in the present study and 5%–14% in bioeroding sponges) (De Bakker et al., 2018)

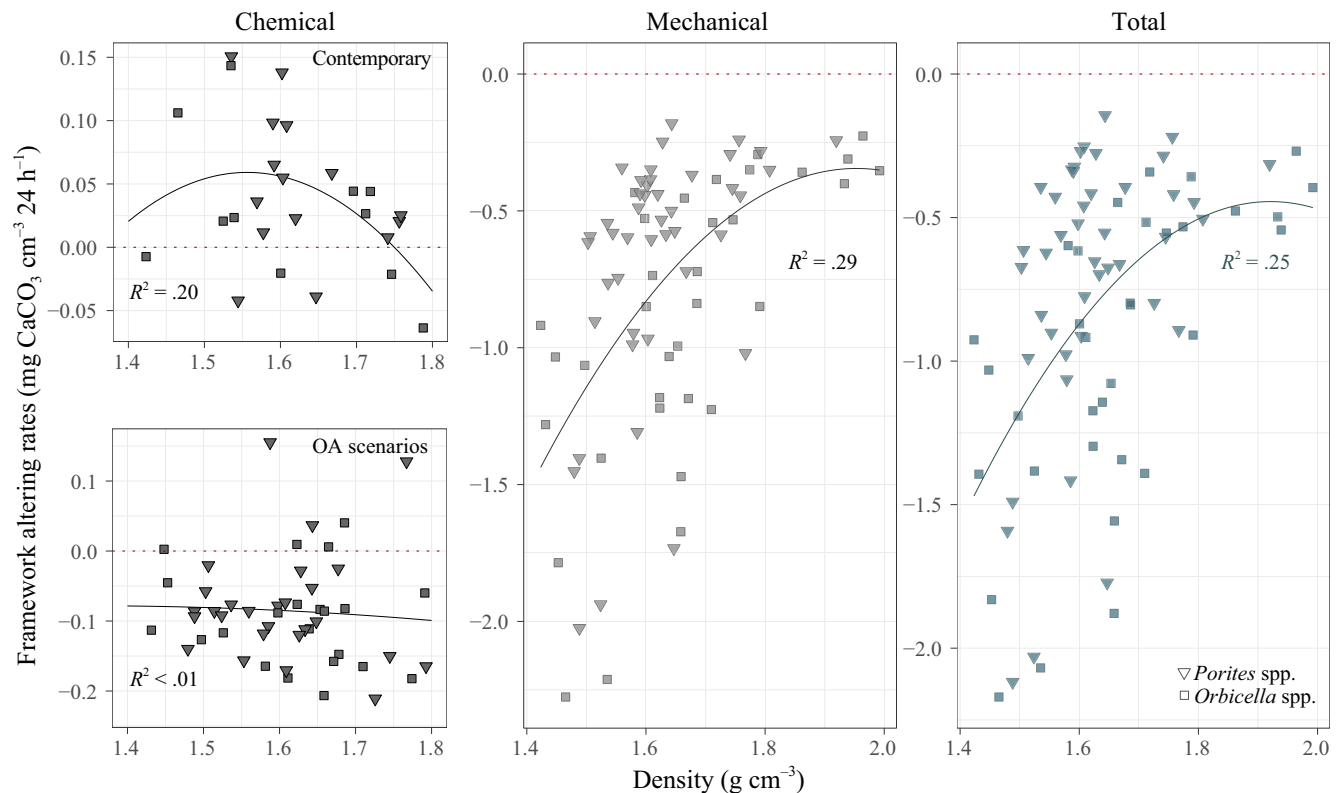


FIGURE 7 Bioerosion and calcification rates in mg CaCO₃ cm⁻³ day⁻¹ as a function of skeletal density in *Porites* spp. (triangles) and *Orbicella* spp. (squares). In the mechanical (grey) and total (blue) bioerosion panels, rates from all three pH scenarios are represented. However, the chemical bioerosion rates (black) in the contemporary scenario are plotted separately from the ocean acidification treatments as the relationship with density is lost in lower pH scenarios.

but it is the way dissolution is utilized to excavate that will ultimately determine if total bioerosion rates are positively or negatively correlated with density. Excavating sponges dissolve the coral skeleton around a CaCO₃ chip to then expel it through their oscula (Webb et al., 2019). No physical scraping or abrasion is utilized in this bio-eroding technique and therefore total erosion (including mechanical) is positively correlated with density. The main boring mechanism of worms and bivalves on the other hand is abrasion (Hutchings, 2008). In this case, mechanical scraping is made easier in less dense substrate and as it contributes to a higher percentage of total bioerosion rates, the latter will be negatively correlated with density.

In the present study, results showed that the relationship between density and rates of bioerosion differed in direction depending on whether the bioerosion was chemical or mechanical in nature. Chemical dissolution was higher in denser skeletons while mechanical rates increased in less dense rubble fragments. Although this relationship held true for mechanical and total rates in all treatments, it did not in OA treatments for chemical rates. This is likely due to water chemistry facilitating dissolution to the point where rubble density has a diminished impact on boring capacity.

Overall, this suggests that density and probably the skeletal structure of corals too (e.g., microskeletal architecture, porosity, and mineralogy) play an important role in determining the magnitude

of the effects of OA on carbonate erosion. Given that OA also induces the formation of lower-density coral structures, we hypothesized that future generations of rubble will support lower density and thus heightened susceptibility to rapid mechanical erosion. OA will therefore both indirectly exert an impact on rates of mechanical bioerosion, and directly enhance rates of chemical dissolution, further deepening the imbalance in favor of net habitat loss (Mollica et al., 2018).

4.3 | Variation in rubble metabolic processes

Due to the different rubble coral species originating from separate sites with distinct environments, it is difficult to disentangle the effect of morphology from location on response rates. It is likely that both the distinct environmental conditions found at the offshore Little Conch and the inshore Cheeca Rocks sites and the different morphologies had an influence on both the micro- and the macro- communities in rubble. For instance, inshore sites in the Florida Keys experience high seasonal variability characterized by periods of exacerbated OA (Palacio-Castro et al., 2023) with implications for the OA sensitivities of organisms establishing there. Previous work on microerosion indicated that distance to the

shore impacted micro-eroder community with microbioerosion increasing offshore (Tribollet et al., 2002; Tribollet & Golubic, 2005). Additionally, higher cryptofaunal abundance has been shown to be linked to surface area to volume ratio with rubble derived from branching coral (e.g., *Acropora*, *Porites*) hosting a greater abundance of organisms than massive coral fragments (e.g., *Orbicella*) (Biondi et al., 2020; Wolfe et al., 2021, 2023). Because the main aim of this research was to quantify the potential overall rubble contribution to daily calcification/dissolution cycling and longer-term bioerosion in future coral reef carbonate budgets, community composition was not the subject of investigation. We can therefore only tentatively infer that the higher variability in NCC and NCP recorded in *Porites* rubble compared to *Orbicella* fragments is a result of more diverse or different community. Whether that is the result of epilithic or endolithic organisms (or both) cannot be said here.

Microbial diversity studies indicate coral rubble's significant role in organic matter decomposition and nutrient recycling, including denitrification and nitrate reduction (Sanchez-Quinto & Falcon, 2021; Sánchez-Quinto & Falcón, 2019). In the present study, both rubble coral species acted as NH_4^+ and NO_3^- sources during the dark in contemporary and elevated treatments. However, results between locations differed during light and dark incubations with *Porites* rubble acting as NO_3^- sinks during the day, while *Orbicella* fragments behaved as sources. The latter is to be

expected from net heterotrophic processes; however, in instances of net autotrophy during the day, rubble acting as net sources of NO_3^- suggest that the consumption and transformation of organic matter by microbial populations (e.g., Pfister & Altabet, 2019) are masking the assimilation of dissolved organic nitrogen by primary producers. This difference found between locations points toward the presence of distinct microbial communities, but further research is needed at this point. In the context of OA, both rubble coral species became net NO_3^- sinks in the high treatment, possibly due to reduced photosynthesis and/or a shift in microbial processes from dominance of nitrification to higher denitrification. The concurrent increase in NH_4^+ release also suggests a shift in microbial processes. There is a scarcity of studies on coral rubble microbial communities and OA. As rubble beds become increasingly common on reefs, determining their role in recycling of organic matter and nutrients in the context of climate change is crucial to understand the increasingly important role they will play on future reefs.

5 | RUBBLE PERSISTENCE AND CONCLUSIONS

The fate of coral rubble on reefs is unknown, especially considering their existence is inherently tied to their source, coral. In

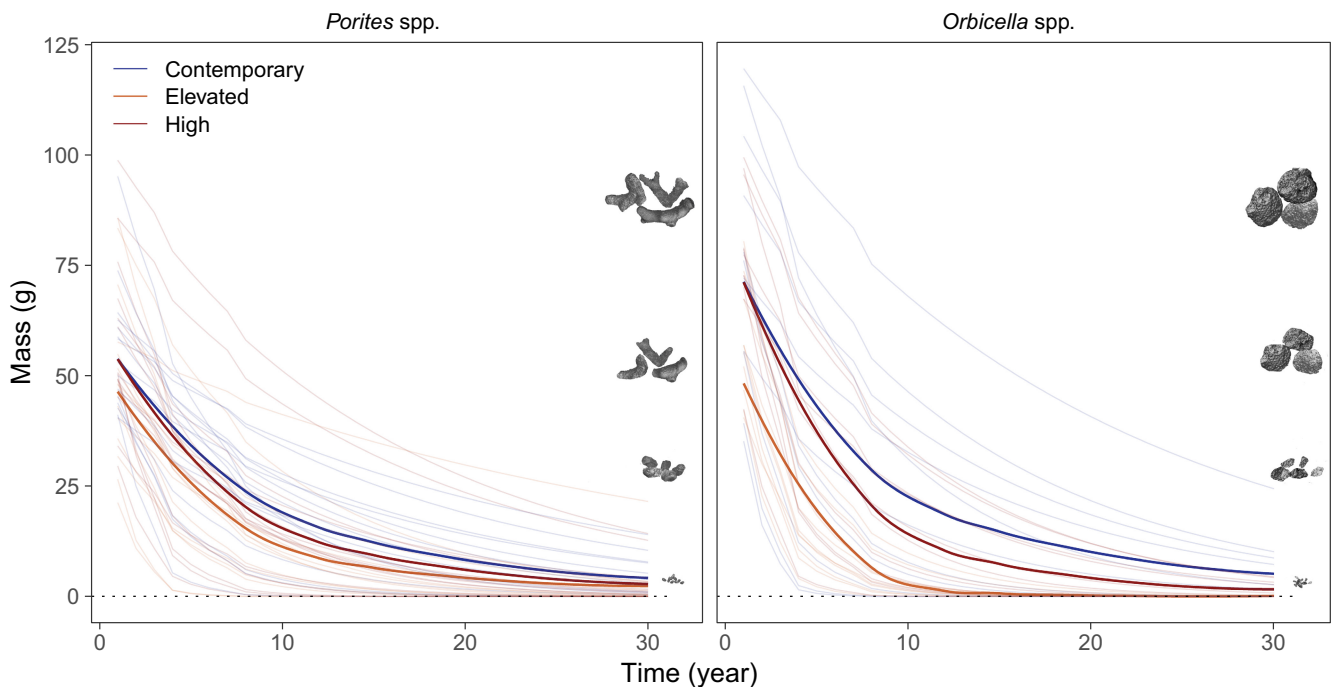


FIGURE 8 Rubble persistence under contemporary, elevated, and high pH treatments. Thin lines represent yearly mass change trajectories for each rubble fragment depending on initial mass, density, volume and respective bioerosion rate measured in this study. Thick lines represent Loess regressions through all rubble fragments from each scenario. See [Supporting Information](#) for yearly mass calculation methods. The change in shape of the rubble scan images depicted on the right side of each panel is purely conjectural, as the extent of their mass loss does not inform their shape alteration. These mass projections do not account for grazing or fracturing resulting from foraging invertebrates or wave action and are therefore likely underestimated.

response to an increased frequency of disturbances on reefs, coral rubble has become a more prevalent substrate component on reef landscapes. Some of this rubble is likely to be reincorporated over time into the reef framework, but in other cases rubble will remain detached from the underlying framework structure and will likely become increasingly mobile as it loses density and weight from bioerosion. This will subject rubble to greater abrasion and physical reworking processes during the transition into sediment grade material (de Kruijf et al., 2021; Kenyon et al., 2020, 2023). By solely considering bioerosion rates from this study, we estimated the approximate time required for the rubble to disintegrate (Figure 8). Differences in rubble persistence between rubble fragments was high, with some fragments disintegrating in under 5 years, while others still weighing more than 10 g after 30 years. On average, rubble mass decreased by more than 70% in less than a decade across all scenarios, before levelling off slowly. This timeframe is likely overestimated as rubble would eventually become so porous that it would fractionate into smaller fragments, accelerating disintegration (Kenyon et al., 2020). *Porites* rubble mass leveled off at around ~10 g after 11 to 13 years in the elevated and high OA scenarios, with a delay of 5 years observed under contemporary pH conditions. *Orbicella* rubble eroded more rapidly in the initial 10 years before slowly plateauing. In the elevated scenario, rubble disintegrated in approximately 10 years. By the 13th year, they decreased to 10 g on average in the high scenario, with an 8-year delay in the contemporary scenario. These rough timelines provide insight on the transition of rubble into sediment grain material. It is worth noting, however, that these rates are not inclusive of grazing or fracturing due to foraging invertivores or wave action which would undoubtedly accelerate the disintegration process (Enochs et al., 2016; Kuffner et al., 2019; Morais et al., 2022).

The high bioerosion rates recorded in this study indicate that dead coral rubble significantly contributes to the carbonate budgets of contemporary disturbed coral reefs, with potential for even greater contributions in the future. OA will both directly enhance rates of chemical dissolution and indirectly promote rates of mechanical bioerosion by impacting the density at which corals form skeleton. These collective impacts will alter the persistence of reef framework, with great repercussions for net reef framework persistence, community structure, and functioning.

AUTHOR CONTRIBUTIONS

Alice E. Webb: Conceptualization; data curation; formal analysis; investigation; methodology; project administration; validation; visualization; writing – original draft; writing – review and editing. **Ana M. Palacio-Castro:** Conceptualization; investigation; methodology; project administration; validation; writing – review and editing. **Kenzie Cooke:** Investigation. **Katherine R. Eaton:** Investigation; writing – review and editing. **Benjamin Chomitz:** Investigation; methodology; writing – review and editing. **Nash Soderberg:** Resources; software. **Morgan Chakraborty:** Investigation. **Zachary**

Zagon: Investigation. **Albert Boyd:** Investigation; resources. **Patrick M. Kiel:** Investigation; software; writing – review and editing. **Allyson DeMerlis:** Investigation. **Chris T. Perry:** Writing – review and editing. **Ian C. Enochs:** Conceptualization; funding acquisition; validation; writing – review and editing.

ACKNOWLEDGMENTS

The authors thank Alexandra Fine and Tyler Christian for nutrient analyses, as well as Nicole Besemer and Graham Kolodziej for their help collecting samples and overseeing equipment management. This work was funded by NOAA's Coral Reef Conservation Program, NOAA's Ocean Acidification Program, and NOAA Omics Initiative.

CONFLICT OF INTEREST STATEMENT

The authors declare no competing interests.

DATA AVAILABILITY STATEMENT

The data that support the findings of this study are openly available in the Dryad data repository at <https://doi.org/10.5061/dryad.pc866t1z8>. CT scan dicom files and orthogonal slice images are available on request from the authors.

ORCID

- Alice E. Webb  <https://orcid.org/0000-0002-6536-6826>
 Katherine R. Eaton  <https://orcid.org/0000-0002-8653-602X>
 Nash Soderberg  <https://orcid.org/0000-0002-3155-4167>
 Zachary Zagon  <https://orcid.org/0009-0001-2432-5630>
 Chris T. Perry  <https://orcid.org/0000-0001-9398-2418>

REFERENCES

- Albright, R., Langdon, C., & Anthony, K. (2013). Dynamics of seawater carbonate chemistry, production, and calcification of a coral reef flat, central Great Barrier Reef. *Biogeosciences*, 10(10), 6747–6758.
 Alvarez-Filip, L., Dulvy, N. K., Gill, J. A., Côté, I. M., & Watkinson, A. R. (2009). Flattening of Caribbean coral reefs: Region-wide declines in architectural complexity. *Proceedings of the Royal Society B: Biological Sciences*, 276(1669), 3019–3025. <https://www.ncbi.nlm.nih.gov/pmc/articles/PMC2817220/pdf/3019.pdf>
 Biondi, P., Masucci, G. D., & Reimer, J. D. (2020). Coral cover and rubble cryptofauna abundance and diversity at outplanted reefs in Okinawa, Japan. *PeerJ*, 8, e9185.
 Brooks, M. E., Kristensen, K., Van Bentem, K. J., Magnusson, A., Berg, C. W., Nielsen, A., Skaug, H. J., Machler, M., & Bolker, B. M. (2017). GLMM tmb balances speed and flexibility among packages for zero-inflated generalized linear mixed modeling. *The R Journal*, 9(2), 378–400.
 Chaves-Fonnegra, A., Riegl, B., Zea, S., Lopez, J. V., Smith, T., Brandt, M., & Gilliam, D. S. (2018). Bleaching events regulate shifts from corals to excavating sponges in algae-dominated reefs. *Global Change Biology*, 24(2), 773–785. <https://doi.org/10.1111/gcb.13962>
 Chisholm, J. R., & Gattuso, J. P. (1991). Validation of the alkalinity anomaly technique for investigating calcification of photosynthesis in coral reef communities. *Limnology and Oceanography*, 36(6), 1232–1239.
 Cosain-Díaz, J. A., Tortolero-Langarica, J. D. J. A., Rodríguez-Troncoso, A. P., Bautista-Guerrero, E., Antuna-Roman, D. M., Salazar-Silva,

- P., & Cupul-Magaña, A. L. (2021). Internal bioerosion in massive corals associated with reef communities in the northeastern tropical Pacific: The effect of intrinsic and extrinsic factors. *Ciencias Marinas*, 47(1), 33–47.
- Davidson, T. M., Altieri, A. H., Ruiz, G. M., & Torchin, M. E. (2018). Bioerosion in a changing world: A conceptual framework. *Ecology Letters*, 21(3), 422–438.
- Davies, P. J., & Hutchings, P. A. (1983). Initial colonization, erosion and accretion of coral substrate: Experimental results, Lizard Island, Great Barrier Reef. *Coral Reefs*, 2, 27–35.
- De Bakker, D. M., Webb, A. E., van den Bogaart, L. A., van Heuven, S. M., Meesters, E. H., & van Duyl, F. C. (2018). Quantification of chemical and mechanical bioerosion rates of six Caribbean excavating sponge species found on the coral reefs of Curaçao. *PLoS One*, 13(5), e0197824. <https://doi.org/10.1371/journal.pone.0197824>
- de Kruijf, M., Slootman, A., de Boer, R. A., & Reijmer, J. J. (2021). On the settling of marine carbonate grains: Review and challenges. *Earth-Science Reviews*, 217, 103532.
- DeCarlo, T. M., Cohen, A. L., Barkley, H. C., Cobban, Q., Young, C., Shamberger, K. E., Brainard, R. E., & Golbuu, Y. (2015). Coral macrobioerosion is accelerated by ocean acidification and nutrients. *Geology*, 43(1), 7–10.
- Dee, S., DeCarlo, T., Ložić, I., Nilsen, J., & Browne, N. K. (2023). Low bioerosion rates on inshore turbid reefs of Western Australia. *Diversity*, 15(1), 62.
- Díaz-Pulido, G., Anthony, K. R., Kline, D. I., Dove, S., & Hoegh-Guldberg, O. (2012). Interactions between ocean acidification and warming on the mortality and dissolution of coralline algae 1. *Journal of Phycology*, 48(1), 32–39.
- Dickson, A. G., Sabine, C. L., & Christian, J. R. (2007). *Guide to best practices for ocean CO₂ measurements*. North Pacific Marine Science Organization.
- Dodge, R. E., Wyers, S. C., Frith, H., Knap, A. H., Smith, S., Cook, C., & Sleeter, T. (1984). Coral calcification rates by the buoyant weight technique: Effects of alizarin staining. *Journal of Experimental Marine Biology and Ecology*, 75(3), 217–232.
- Enochs, I., Manzello, D., Jones, P., Aguilar, C., Cohen, K., Valentino, L., Schopmeyer, S., Kolodziej, G., Jankulak, M., & Lirman, D. (2018). The influence of diel carbonate chemistry fluctuations on the calcification rate of *Acropora cervicornis* under present day and future acidification conditions. *Journal of Experimental Marine Biology and Ecology*, 506, 135–143.
- Enochs, I. C., & Manzello, D. P. (2012). Responses of cryptofaunal species richness and trophic potential to coral reef habitat degradation. *Diversity*, 4(1), 94–104.
- Enochs, I. C., Manzello, D. P., Kolodziej, G., Noonan, S. H., Valentino, L., & Fabricius, K. E. (2016). Enhanced macropore and depressed calcification drive net dissolution at high-CO₂ coral reefs. *Proceedings of the Royal Society B: Biological Sciences*, 283(1842), 20161742.
- Enochs, I. C., Toth, L. T., Kirkland, A., Manzello, D. P., Kolodziej, G., Morris, J. T., Holstein, D. M., Schlenz, A., Randall, C. J., & Mate, J. L. (2021). Upwelling and the persistence of coral-reef frameworks in the eastern tropical Pacific. *Ecological Monographs*, 91(4), e01482.
- Ferrario, F., Beck, M. W., Storlazzi, C. D., Micheli, F., Shepard, C. C., & Airolidi, L. (2014). The effectiveness of coral reefs for coastal hazard risk reduction and adaptation. *Nature Communications*, 5(1), 3794.
- Gattuso, J.-P., Epitalon, J.-M., Lavigne, H., Orr, J., Gentili, B., Hagens, M., Hofmann, A., Mueller, J.-D., Proye, A., & Rae, J. (2015). Package 'seacarb'. <http://cran.r-project.org/package=seacarb>
- Glynn, P. W., & Manzello, D. P. (2015). Bioerosion and coral reef growth: A dynamic balance. In C. Birkeland (Ed.), *Coral reefs in the Anthropocene* (pp. 67–97). Springer.
- Graham, N. A., & Nash, K. L. (2013). The importance of structural complexity in coral reef ecosystems. *Coral Reefs*, 32, 315–326.
- Groves, S. H., Holstein, D. M., Enoch, I. C., Kolodziej, G., Manzello, D. P., Brandt, M. E., & Smith, T. B. (2018). Growth rates of *Porites* astreoides and *Orbicella franksi* in mesophotic habitats surrounding St. Thomas, US Virgin Islands. *Coral Reefs*, 37, 345–354.
- Hartig, F. (2020). DHARMA: Residual diagnostics for hierarchical (multi-level/mixed) regression models. *R package v0.2.0*.
- Hernández-Ballesteros, L. M., Elizalde-Rendón, E. M., Carballo, J. L., & Carricart-Ganivet, J. P. (2013). Sponge bioerosion on reef-building corals: Dependent on the environment or on skeletal density? *Journal of Experimental Marine Biology and Ecology*, 441, 23–27.
- Highsmith, R. C. (1981). Coral bioerosion: damage relative to skeletal density. *The American Naturalist*, 117(2), 193–198.
- Highsmith, R. C., Lueptow, R. L., & Schonberg, S. C. (1983). Growth and bioerosion of three massive corals on the Belize barrier reef. *Marine ecology progress series*. Oldendorf, 13(2), 261–271.
- Holmes, K. E. (2000). Effects of eutrophication on bioeroding sponge communities with the description of new West Indian sponges, *Cliona* spp. (Porifera: Hadromerida: Clionidae). *Invertebrate Biology*, 119(2), 125–138.
- Hughes, T. P., Kerry, J. T., Baird, A. H., Connolly, S. R., Dietzel, A., Eakin, C. M., Heron, S. F., Hoey, A. S., Hoogenboom, M. O., & Liu, G. (2018). Global warming transforms coral reef assemblages. *Nature*, 556(7702), 492–496.
- Hutchings, P. (1986). Biological destruction of coral reefs: A review. *Coral Reefs*, 4, 239–252.
- Hutchings, P. (2008). Role of polychaetes in bioerosion of coral substrates. In M. Wissak, & L. Tapanila (Eds.), *Current developments in bioerosion*, Erlangen Earth Conference Series (pp. 249–264). Springer.
- Jacques, T., & Pilson, M. (1980). Experimental ecology of the temperate scleractinian coral *Astrangia danae* I. Partition of respiration, photosynthesis and calcification between host and symbionts. *Marine Biology*, 60, 167–178.
- Kenyon, T. M., Doropoulos, C., Dove, S., Webb, G. E., Newman, S. P., Sim, C. W., Arzan, M., & Mumby, P. J. (2020). The effects of rubble mobilisation on coral fragment survival, partial mortality and growth. *Journal of Experimental Marine Biology and Ecology*, 533, 151467.
- Kenyon, T. M., Harris, D., Baldock, T., Callaghan, D., Doropoulos, C., Webb, G., Newman, S. P., & Mumby, P. J. (2023). Mobilisation thresholds for coral rubble and consequences for windows of reef recovery. *Biogeosciences Discussions*, 2023, 1–28.
- Kiene, W., & Hutchings, P. (1994). Bioerosion experiments at Lizard Island, Great Barrier Reef. *Coral Reefs*, 13, 91–98.
- Kline, D. I., Teneva, L., Okamoto, D. K., Schneider, K., Caldeira, K., Miard, T., Chai, A., Marker, M., Dunbar, R. B., & Mitchell, B. G. (2019). Living coral tissue slows skeletal dissolution related to ocean acidification. *Nature Ecology & Evolution*, 3(10), 1438–1444.
- Kuffner, I. B., Andersson, A. J., Jokiel, P. L., Rodgers, K. U. S., & Mackenzie, F. T. (2008). Decreased abundance of crustose coralline algae due to ocean acidification. *Nature Geoscience*, 1(2), 114–117.
- Kuffner, I. B., Toth, L. T., Hudson, J. H., Goodwin, W. B., Stathakopoulos, A., Bartlett, L. A., & Whitcher, E. M. (2019). Improving estimates of coral reef construction and erosion with in situ measurements. *Limnology and Oceanography*, 64(5), 2283–2294.
- Manzello, D. P., Enoch, I. C., Kolodziej, G., Carlton, R., & Valentino, L. (2018). Resilience in carbonate production despite three coral bleaching events in 5 years on an inshore patch reef in the Florida Keys. *Marine Biology*, 165, 1–11.
- Manzello, D. P., Kolodziej, G., Kirkland, A., Besemer, N., & Enoch, I. C. (2021). Increasing coral calcification in *Orbicella faveolata* and *Pseudodiploria strigosa* at Flower Garden Banks, Gulf of Mexico. *Coral Reefs*, 40(4), 1097–1111.
- Molina-Hernández, A., González-Barrios, F. J., Perry, C. T., & Álvarez-Filip, L. (2020). Two decades of carbonate budget change on shifted coral reef assemblages: Are these reefs being locked into low net budget states? *Proceedings of the Royal Society B*, 287(1940), 20202305. <https://www.ncbi.nlm.nih.gov/pmc/articles/PMC7739932/pdf/rspb20202305.pdf>

- Molina-Hernández, A., Medellín-Maldonado, F., Lange, I. D., Perry, C. T., & Alvarez-Filip, L. (2022). Coral reef erosion: In situ measurement on different dead coral substrates on a Caribbean reef. *Limnology and Oceanography*, 67, 2734–2749.
- Mollica, N. R., Guo, W., Cohen, A. L., Huang, K.-F., Foster, G. L., Donald, H. K., & Solow, A. R. (2018). Ocean acidification affects coral growth by reducing skeletal density. *Proceedings of the National Academy of Sciences of the United States of America*, 115(8), 1754–1759.
- Morais, J., Morais, R., Tebbett, S. B., & Bellwood, D. R. (2022). On the fate of dead coral colonies. *Functional Ecology*, 36(12), 3148–3160.
- Morris, J. T., Enochs, I. C., Besemer, N., Viehman, T. S., Groves, S. H., Blondeau, J., Ames, C., Towle, E. K., Grove, L. J. W., & Manzello, D. P. (2022). Low net carbonate accretion characterizes Florida's coral reef. *Scientific Reports*, 12(1), 19582. <https://www.nature.com/articles/s41598-022-23394-4.pdf>
- Osorno, A., Peyrot-Clausade, M., & Hutchings, P. (2005). Patterns and rates of erosion in dead Porites across the Great Barrier Reef (Australia) after 2 years and 4 years of exposure. *Coral Reefs*, 24, 292–303.
- Palacio-Castro, A., Enochs, I., Besemer, N., Boyd, A., Jankulak, M., Kolodziej, G., Hirsh, H., Webb, A., Towle, E., & Kelble, C. (2023). Coral reef carbonate chemistry reveals interannual, seasonal, and spatial impacts on ocean acidification off Florida. *Global Biogeochemical Cycles*, 37(12), e2023GB007789.
- Perry, C. T., Alvarez-Filip, L., Graham, N. A., Mumby, P. J., Wilson, S. K., Kench, P. S., Manzello, D. P., Morgan, K. M., Slangen, A., & Thomson, D. P. (2018). Loss of coral reef growth capacity to track future increases in sea level. *Nature*, 558(7710), 396–400. <https://www.nature.com/articles/s41586-018-0194-z.pdf>
- Perry, C. T., & Hepburn, L. (2008). Syn-depositional alteration of coral reef framework through bioerosion, encrustation and cementation: Taphonomic signatures of reef accretion and reef depositional events. *Earth-Science Reviews*, 86(1–4), 106–144.
- Perry, C. T., Murphy, G. N., Kench, P. S., Smithers, S. G., Edinger, E. N., Steneck, R. S., & Mumby, P. J. (2013). Caribbean-wide decline in carbonate production threatens coral reef growth. *Nature Communications*, 4(1), 1402.
- Perry, C. T., Spencer, T., & Kench, P. (2008). Carbonate budgets and reef production states: A geomorphic perspective on the ecological phase-shift concept. *Coral Reefs*, 27, 853–866.
- Pfister, C. A., & Altabet, M. A. (2019). Enhanced microbial nitrogen transformations in association with macrobiota from the rocky intertidal. *Biogeosciences*, 16(2), 193–206.
- Pörtner, H.-O., Roberts, D. C., Masson-Delmotte, V., Zhai, P., Tignor, M., Poloczanska, E., & Weyér, N. (2019). *The ocean and cryosphere in a changing climate*. IPCC special report on the ocean and cryosphere in a changing climate, 1155.
- R Core Team. (2023). R: A language and environment for statistical computing. R Foundation for Statistical Computing, Vienna, Austria. <https://www.R-project.org>
- Rasser, M., & Riegl, B. (2002). Holocene coral reef rubble and its binding agents. *Coral Reefs*, 21, 57–72.
- Riahi, K., Van Vuuren, D. P., Kriegler, E., Edmonds, J., O'Neill, B. C., Fujimori, S., Bauer, N., Calvin, K., Dellink, R., & Fricko, O. (2017). The shared socioeconomic pathways and their energy, land use, and greenhouse gas emissions implications: An overview. *Global Environmental Change*, 42, 153–168.
- Rogers, A., Blanchard, J. L., & Mumby, P. J. (2018). Fisheries productivity under progressive coral reef degradation. *Journal of Applied Ecology*, 55(3), 1041–1049.
- Romanó de Orte, M., Koweek, D. A., Cyronak, T., Takeshita, Y., Griffin, A., Wolfe, K., Szmant, A., Whitehead, R., Albright, R., & Caldeira, K. (2021). Unexpected role of communities colonizing dead coral substrate in the calcification of coral reefs. *Limnology and Oceanography*, 66(5), 1793–1803.
- Sánchez-Quinto, A., & Falcón, L. I. (2019). Metagenome of Acropora palmata coral rubble: Potential metabolic pathways and diversity in the reef ecosystem. *PLoS One*, 14(8), e0220117.
- Sanchez-Quinto, A., & Falcon, L. I. (2021). Formation and metabolic function of coral rubble biofilms in the reef ecosystem. *Gulf and Caribbean Research*, 32(1), 46–56.
- Schönberg, C. H., Fang, J. K., Carreiro-Silva, M., Tribollet, A., & Wissahak, M. (2017). Bioerosion: The other ocean acidification problem. *ICES Journal of Marine Science*, 74(4), 895–925.
- Scoffin, T. (1992). Taphonomy of coral reefs: A review. *Coral Reefs*, 11, 57–77.
- Silbiger, N., & Donahue, M. (2015). Secondary calcification and dissolution respond differently to future ocean conditions. *Biogeosciences*, 12(2), 567–578.
- Smith, S., & Key, G. (1975). Carbon dioxide and metabolism in marine environments 1. *Limnology and Oceanography*, 20(3), 493–495.
- Spencer Davies, P. (1989). Short-term growth measurements of corals using an accurate buoyant weighing technique. *Marine Biology*, 101, 389–395.
- Stubler, A. D., & Peterson, B. J. (2016). Ocean acidification accelerates net calcium carbonate loss in a coral rubble community. *Coral Reefs*, 35, 795–803.
- Tribollet, A., Decherf, G., Hutchings, P., & Peyrot-Clausade, M. (2002). Large-scale spatial variability in bioerosion of experimental coral substrates on the Great Barrier Reef (Australia): Importance of microborers. *Coral Reefs*, 21, 424–432.
- Tribollet, A., & Golubic, S. (2005). Cross-shelf differences in the pattern and pace of bioerosion of experimental carbonate substrates exposed for 3 years on the northern Great Barrier Reef, Australia. *Coral Reefs*, 24, 422–434.
- van Hoidonk, R., Maynard, J., Grimsditch, G., Williams, G., Tamelander, J., Gove, J., Koldewey, H., Ahmadia, G., Tracey, D., & Hum, K. (2020). Citation: UNEP 2020. *Projections of future coral bleaching conditions using IPCC CMIP6 models: Climate policy implications, management applications, and Regional Seas summaries*. UNEP.
- Webb, A. E., Enochs, I. C., van Hoidonk, R., van Westen, R. M., Besemer, N., Kolodziej, G., Viehman, T. S., & Manzello, D. P. (2023). Restoration and coral adaptation delay, but do not prevent, climate-driven reef framework erosion of an inshore site in the Florida Keys. *Scientific Reports*, 13(1), 258. <https://www.nature.com/articles/s41598-022-26930-4.pdf>
- Webb, A. E., Pomponi, S. A., van Duyl, F. C., Reichart, G.-J., & de Nooijer, L. J. (2019). pH regulation and tissue coordination pathways promote calcium carbonate bioerosion by excavating sponges. *Scientific Reports*, 9(1), 758.
- Webb, A. E., van Heuven, S. M., de Bakker, D. M., van Duyl, F. C., Reichart, G.-J., & de Nooijer, L. J. (2017). Combined effects of experimental acidification and eutrophication on reef sponge bioerosion rates. *Frontiers in Marine Science*, 4, 311.
- Wissahak, M., Schönberg, C. H., Form, A., & Freiwald, A. (2013). Effects of ocean acidification and global warming on reef bioerosion lessons from a clionaid sponge. *Aquatic Biology*, 19(2), 111–127.
- Wolfe, K., Kenyon, T. M., Desbiens, A., de la Motte, K., & Mumby, P. J. (2023). Hierarchical drivers of cryptic biodiversity on coral reefs. *Ecological Monographs*, 93(3), e1586.
- Wolfe, K., Kenyon, T. M., & Mumby, P. J. (2021). The biology and ecology of coral rubble and implications for the future of coral reefs. *Coral Reefs*, 40, 1769–1806.
- Wolff, N. H., Mumby, P. J., Devlin, M., & Anthony, K. R. (2018). Vulnerability of the Great Barrier Reef to climate change and local pressures. *Global Change Biology*, 24(5), 1978–1991.
- Yates, K., & Halley, R. (2006). CO_3^{2-} concentration and pCO_2 thresholds for calcification and dissolution on the Molokai reef flat, Hawaii. *Biogeosciences*, 3(3), 357–369.

- Yates, K. K., Zawada, D. G., Smiley, N. A., & Tiling-Range, G. (2017). Divergence of seafloor elevation and sea level rise in coral reef ecosystems. *Biogeosciences*, 14(6), 1739–1772.
- Yeung, Y. H., Xie, J. Y., Zhao, Y., Yu, H. Y., Chen, C., Lu, W. W., & Qiu, J.-W. (2021). Rapid external erosion of coral substrate in subtropical Hong Kong waters. *Marine Pollution Bulletin*, 169, 112495.
- Zundelevich, A., Lazar, B., & Ilan, M. (2007). Chemical versus mechanical bioerosion of coral reefs by boring sponges—lessons from *Pione cf. vastifica*. *Journal of Experimental Biology*, 210(1), 91–96.

SUPPORTING INFORMATION

Additional supporting information can be found online in the Supporting Information section at the end of this article.

How to cite this article: Webb, A. E., Palacio-Castro, A. M., Cooke, K., Eaton, K. R., Chomitz, B., Soderberg, N., Chakraborty, M., Zagon, Z., Boyd, A., Kiel, P. M., DeMerlis, A., Perry, C. T., & Enochs, I. C. (2024). Rubble persistence under ocean acidification threatened by accelerated bioerosion and lower-density coral skeletons. *Global Change Biology*, 30, e17371. <https://doi.org/10.1111/gcb.17371>